A Monolithically Integrated Electronic-Photonic Front-end Utilizing Micro-ring Modulators for Large-Scale mm-wave Sensing

Ruocheng Wang[1], Manuj Singh[2], Deniz Onural[2], Sidney Buchbinder[1], Hayk Gevorgyan[2], Miloš A. Popović[2], Vladimir Stojanović[1],
[1]*Department of Electrical Engineering and Computer Sciences, UC Berkeley, Berkeley, USA*
[2]*Department of Electrical and Computer Engineering, Photonics Center, Boston University, Boston, USA*

***Abstract*—This work presents a fully-integrated electronic-photonic mm-wave sensing element, fabricated in a commercial 45 nm SOI process. The sensing element features a low-noise amplifier (LNA) tuned to drive an integrated electro-optical micro-ring modulator (MRM) instead of conventional Mach-Zehnder modulator (MZM) with a large footprint. With sensing element power of only 30 mW and area of 0.6 mm^2, the design enables compact, low-power mm-wave sensor arrays with thousands of elements, paving the way to new distributed sensing and cell-free radio architectures. The mm-wave sensing element reaches a sideband conversion efficiency (SCE) saturation point at around -35 dBm of received RF power, and achieves a peak SCE of -49.5 dB with -45 dBm received RF power and incident laser power up to 4 dBm over 2GHz of RF bandwidth centered at 57GHz, which projects to a link noise figure of 20.6 dB with 9 dBm total laser power.**

***Index Terms*—silicon photonics, massive MIMO, micro ring modulator**

I. Introduction

Utilizing higher frequency bands (50 - 100 GHz and beyond) enables thousands of antenna elements per array panel for future communication and sensing systems, but brings unique challenges in size, weight, power and cost (SWAP-C). With increases in carrier frequency, both the channel bandwidth and number of antennas increase leading to a quadratic increase in the number of baseband samples and in beamforming compute throughput. This causes both the beamforming processors and the links from ADCs / DACs to processors to begin dominating the SWAP-C of the array panel. Emerging high-density, low-power silicon-photonic optical links directly from ADC / DAC or RFIC chips would enable radio unit (RU) disaggregation into a low SWAP-C sensor panel and remote processor. This further enables new multi-static sensing and cell-free communication architectures where many low SWAP-C panels per central processing site can be organized to optimize the sensing and communication capacity.

In this paper we describe the design of a compact, low-power mm-wave sensing element, consisting of an LNA driver monolithically integrated with a silicon-photonic single-ring MRM [1]. This design is a key building block that enables implementation of low SWAP-C mm-wave sensing arrays with thousands of sensing elements, as illustrated in Figure 1.

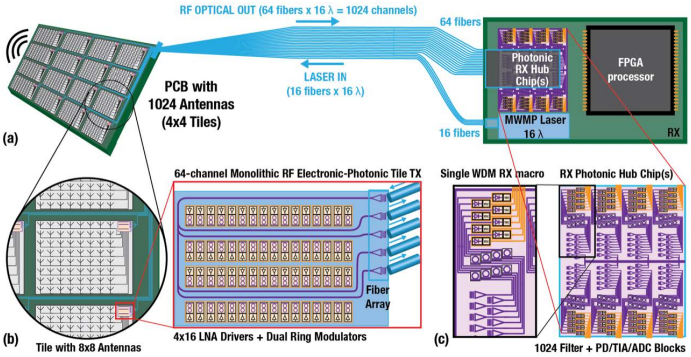

Fig. 1: Diagram of the proposed system architecture

The array site communicates with the processing hub via photonic links. The photonic links feature wavelength division multiplexing (WDM), which reduces the number of physical channels, and take advantage of lower crosstalk and loss along the link channel. While providing the high-bandwidth connectivity to the remote processing hub, the design leverages the small MRM size (with 10 µm diameter and ∼10 fF capacitance, typically 100 times smaller area and power footprint than MZM), monolithic integration with LNA driver, and wavelength-multiplexing capability to realize energy-efficient, high-bandwidth density transmission.

II. Photonic Transmitter Design

A. Link Architecture

The architecture of the proposed photonic link connecting a mm-wave sensing element to a remote processing hub is shown in Figure 2. The mm-wave sensing element (photonic Tx) demonstrated in this work consists of a mm-wave LNA driver, tuned to drive the MRM monolithically integrated on the same chip. The comb laser source with tone spacing (f_{LO}) sends a pump tone at frequency f_1 to the photonic Tx, while sending the reference tone at frequency $f_2 = f_1 + f_{LO}$ to the photonic Rx. The LNA receives the mm-wave signal from the antenna and drives the MRM with the amplified signal. The MRM is an electro-optic (EO) modulator which modulates magnitude and phase of the laser at its through port by the voltage applied to its electrodes. The modulation creates an

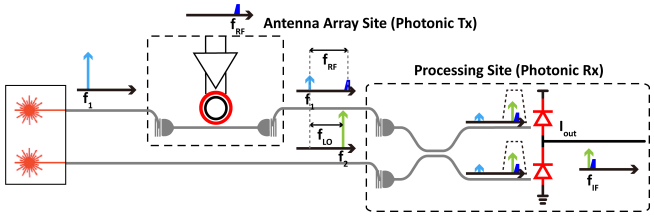

Fig. 2: Diagram of the link

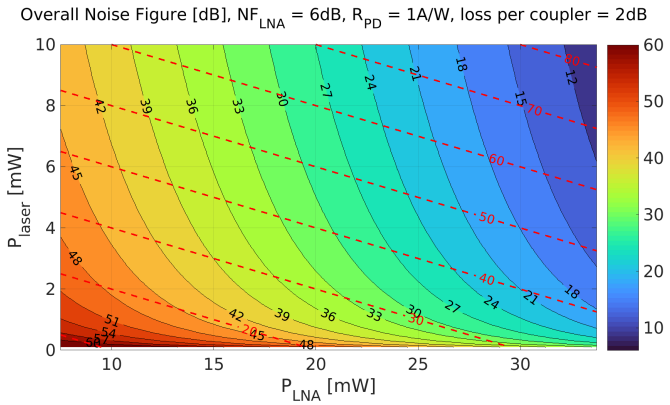

Fig. 3: Contours v.s. LNA power and total optical power. Colored map: link NF [dB]; red dashed lines: total power [mW] (LNA power + laser source wall-plug power)

optical sideband with the same spectrum as the RF modulation signal (see Figure 2). The RF/mm-wave signal driving the MRM generates an optical sideband located f_{RF} away from the pump tone at f_1, which is close to the reference tone at f_2. On the processing site (photonic Rx), the sideband is combined with the reference laser tone through an optical 2×2 coupler and down-converted to electrical photocurrent signal centered at $f_{RF} - f_{LO}$, through the balanced photodetector (PD), then processed by the rest of the receiver front-end. This architecture is similar to the laser-forwarded coherent link [2] which fundamentally avoids some of the coupling loss, while an additional tone is introduced here to realize the RF/mm-wave signal down-conversion to IF.

B. Link Modeling and LNA Design

Suppose the signal sideband power reaching the photonic Rx is P_{sig}, the reference power is P_{ref}, and assume that $P_{ref} \gg P_{sig}$. The total DC current that creates the shot noise and the AC current will be:

$$I_{shot} = \Re_{PD}(P_{sig} + P_{ref}) \approx \Re_{PD}P_{ref} \tag{1}$$

$$i_{AC} = 2\Re_{PD}\sqrt{P_{sig}P_{ref}} \tag{2}$$

where $\Re_{PD}$ is the responsivity of the photodetector (PD). This already gives intuition on the relation between the output SNR and the design parameter, since if we only consider the shot noise at the PD, we have:

$$\frac{i_{AC}^2/2}{\overline{i_n^2}} = \frac{2\Re_{PD}^2 P_{sig}P_{ref}}{2qB\cdot\Re_{PD}P_{ref}} = \frac{\Re_{PD}P_{sig}}{qB} = \frac{\Re_{PD}c_{SCE}P_{pump}}{qB}. \tag{3}$$

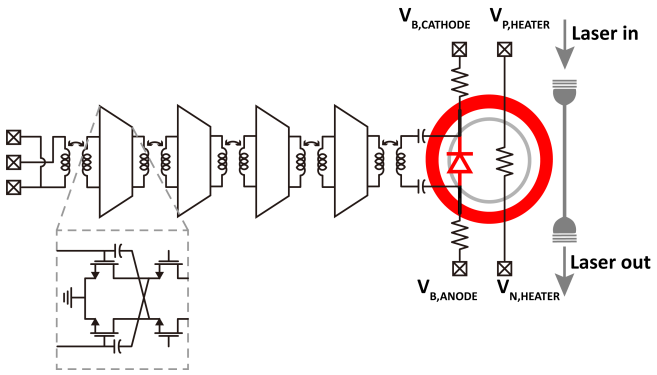

Fig. 4: Schematic of the LNA with its implementation in the Tx array element

Here B is the signal bandwidth, and we define the c_{SCE} parameter as sideband conversion efficiency (SCE), which is the ratio of the sideband power to the incident laser power reaching the ring. The SCE depends on intrinsic performance of the MRM like the resonance shift per volt, the optical cavity Q, and the voltage applied to its electrodes. In practice, P_{pump} is close to P_{ref} (both generated from wavelength components of a laser comb), so the overall gain and noise performance of this link depend on: 1) the laser power reaching the PD, which takes the insertion loss of the photonics into account, e.g. that of the waveguide, the coupler and the modulator, 2) the PD responsivity, 3) the SCE of the modulator that may be driven by an amplifier, as is the case here, or directly driven by the RF signal from the antenna. While on the photonic side various novel MRMs [3, 4] have been created with improved SCE for band-limited RF signals compared to single-ring MRMs, the noise figure (NF) is still very high to date, indicating the need for a preamplifier. A behavioral model is developed to achieve the target NF, shown in Fig. 3. The model assumes that the LNA has a high power gain to enhance the SCE of the LNA-MRM chain, and based on the assumption that the LNA consists of multiple cascaded gain stages, its total power is proportional to its gain in dB. The red dashed lines in Fig. 3 represent contours of constant total power, which is the sum of the LNA power and the electrical wall-plug power of the laser source assuming 20% wall-plug efficiency (WPE). Together with the NF contours, it shows the optimal design point corresponding to a given total power or a specific NF. In practice, several other factors apply additional constraints on the design space: the LNA gain is limited by linearity and output SNR design specifications; the P_{pump} is limited by the input power into the MRM (since excessive power affects the stability and SCE of the MRM due to self-heating), and the P_{ref} is constrained by the input power limit of the photodetector.

III. Measurement Results

In this design, a differential LNA shown in Fig. 4 is designed to drive the MRM in a push-pull mode, which can also be used to drive the novel MRMs in [3],[4]. The LNA consists of multiple cascaded stages with differential pairs and transformers to

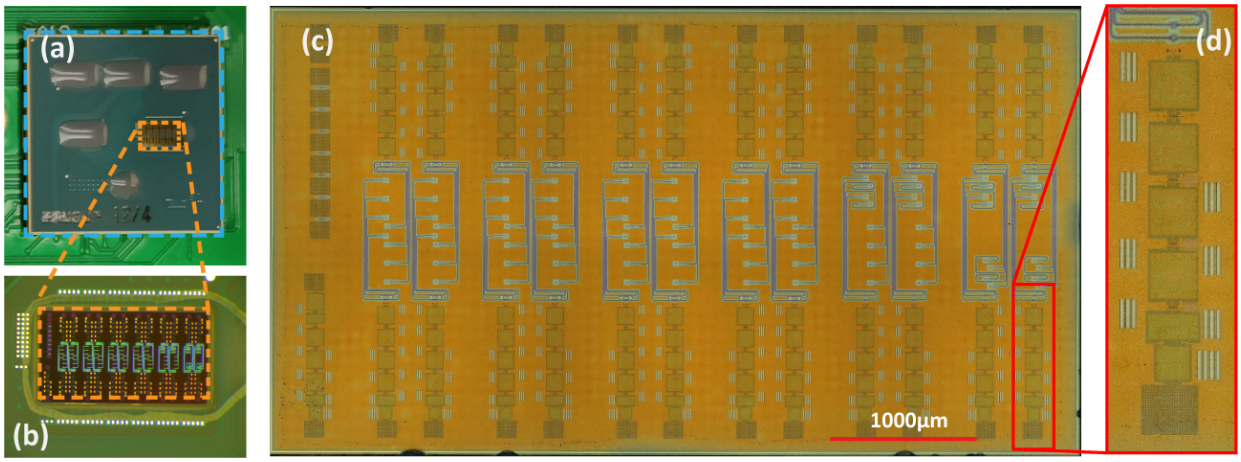

Fig. 5: (a) Packaged organic substrate on the host board (b) Substrate released chip with the package (c) Micrograph of the whole chip (d) LNA+single-ring MRM test-site inset

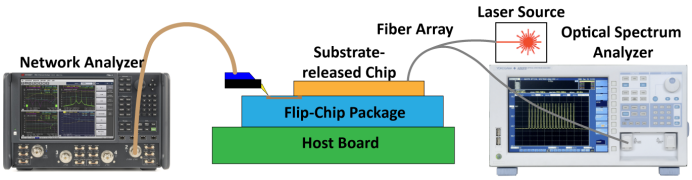

Fig. 6: Experimental setup

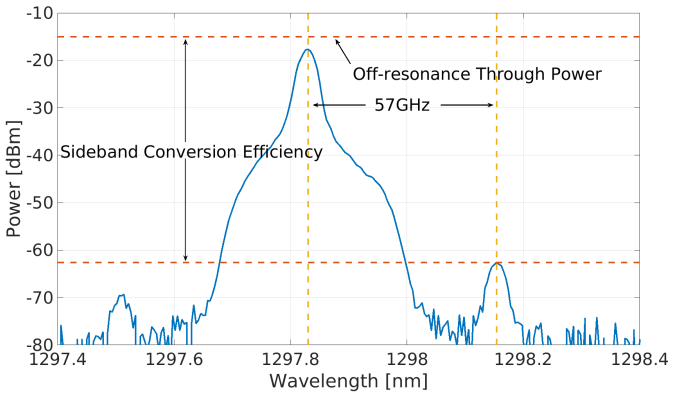

Fig. 7: Spectrum reaching the OSA

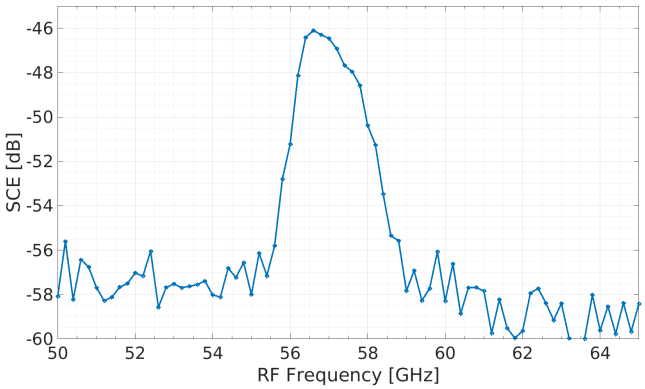

Fig. 8: Sideband conversion efficiency v.s. RF frequency

provide ∼10 dB of gain per stage. For each stage, the common-source differential pair has neutralization capacitors to reduce the input capacitance and signal reflection, and common-gate transistors are implemented to further increase the power gain. An on-chip balun with impedance matching is implemented at the input to accommodate a single-ended RF signal, and the output of the LNA is matched to the impedance of the ring modulator. The LNA is designed to have a power gain of 40 dB, with a noise figure of 6 dB.

The photonic Tx chip is fabricated in a 45 nm RFSOI CMOS process. The silicon substrate layer of the chip underneath the SiO_2 buried oxide is etched away to enable low loss optical mode (after the chip is flip-chip packaged on an organic substrate). The package and the die micrograph of a substrate-released sample are shown in Figure 5. In the measurement setup, a fiber array is attached from the removed substrate side to the chip, which couples the continuous wave (CW) laser LO into the chip, and also couples the optical signal at the through-port of the MRM out of the chip to an optical spectrum analyzer (OSA), shown in Fig. 6. The mm-wave signal at f_{RF} amplified by the on-chip LNA modulates the MRM and generates an optical sideband f_{RF} away from the CW laser signal, as shown in Figure 7.

Figures 7-10 show experimental results for SCE of the LNA driving the single-ring MRM as a function of input RF power, RF frequency and input laser power, as well as the estimated noise figure of the mm-wave link in Figure 2. Figure 7 shows the modulated spectrum with a sideband with off-resonance power level marked as well. With improved coupling conditions, the coupling loss can be reduced from 15dB in the experiment to around 4 dB, i.e. 2 dB per coupler. Figure 8 shows the SCE as a function of RF frequency, with the ∼2 GHz "passband" set by the LNA. Figure 9 illustrates the relationship between SCE and the RF power, where no significant performance degradation from self-heating of the ring occurs up to 4 dBm ring incident optical power. The plot also shows the link begins to saturate around -35 dBm input RF power. The measured SCE matches the theoretical model, and is mainly limited by the RC bandwidth and the relatively

TABLE I: Comparison with State-of-the-Art RF Photonic Modulators/Front-ends

Reference	This work	*Fio+LS 2019* [3]	*JLT 2023*[5]		*RFIC 2019*[6]
Monolithic Integration	Yes	NA	NA[#]	No[*]	No
Driver Process	45nm SOI	NA	NA	Discrete	130nm SiGe BiCMOS
Electrical Power [mW]	30[‖]	-	-	5000	1700
Optical Modulator	MRM	Dual MRM	MZM	MZM	MZM
SCE [dB]	-49.5 @ -45dBm P_{RF}	-42 @ -20dBm P_{RF}	-	-	-
Laser Power [dBm]	9	9	4.8	30	-
NF [dB]	20.6[§] @ 57GHz	37.9[§] @ 41GHz	43 @ 20GHz	11.1 @ 20GHz	20 @20GHz

[‖]heater tuning power up to 16mW excluded [#]without EDFA or pre-amplifier
[*]with 2 EDFAs and 1 pre-amplifier, output power of the EDFA is taken as a laser source power
[§]projected NF assuming 9dBm total laser power and 2dB loss per coupler (4dBm incident power at the MRM)

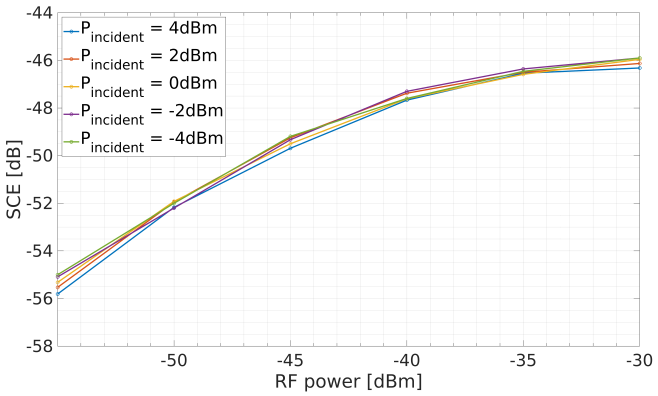

Fig. 9: Sideband conversion efficiency v.s. RF power

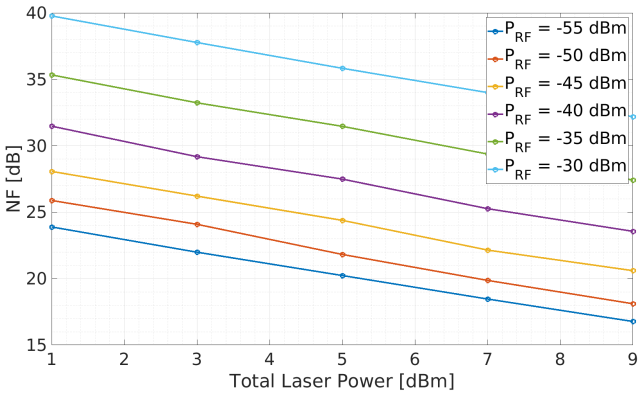

Fig. 10: Projected NF v.s. total laser power, 2dB loss per coupler

low quality factor of the single-ring MRM variant measured so far. The noise figure of LNA+single-ring MRM is still comparable to that of a standalone dual-ring modulator [3], which intrinsically has better SCE than the standalone single-ring MRM tested in this LNA+single-ring MRM experiment. Hence, the performance of the proposed architecture can be further improved by integrating the LNA with these more efficient MRMs. Table I compares this design with previous work focused on MZMs, illustrating that smaller footprint and power per element as well as higher modulation frequency are achievable with pre-amplified MRM designs, owing to the large load capacitance and area of the MZM designs. The resonant nature of MRMs also enables wavelength division multiplexing compared to broadband MZM designs, enabling scaling to larger arrays due to more sensing elements per fiber. The power consumption per array element is 30 mW from the LNA, which shows that thousands of such elements can be integrated in a low-power mm-wave sensing array.

Conclusion

A silicon-photonic link architecture is proposed for large scale massive-MIMO mm-wave signal aggregation and processing. The architecture takes advantage of WDM which reduces the physical channel footprint for massive scale signal communication. The fully integrated monolithic mm-wave sensing element can achieve a noise figure of around 20.6 dB with less than 30 mW of power per element, which can be further improved by applying advanced MRMs with higher electrical bandwidth and superior conversion efficiency.

Acknowledgment

This work was funded by the US Government. We would like to thank Ayar Labs for their support related to the 45RF process. The chips were fabricated by GlobalFoundries

References

[1] Hayk Gevorgyan et al. “High Shift Efficiency O-band Spoked-Ring Modulator Allowing Fully Electro-Optic Channel Tuning in a 45nm CMOS Platform”. In: *Conference on Lasers and Electro-Optics*. Optica Publishing Group, 2021, SW3C.5.

[2] Nandish Mehta et al. “A Laser-Forwarded Coherent Transceiver in 45-nm SOI CMOS Using Monolithic Microring Resonators”. In: *IEEE Journal of Solid-State Circuits* 55.4 (2020), pp. 1096–1107.

[3] Hayk Gevorgyan, Anatol Khilo, and Miloš A. Popović. “Efficient coupled-cavity electro-optic modulator on silicon for high carrier frequency, narrowband RF signals”. In: *Frontiers in Optics + Laser Science APS/DLS*. Optica Publishing Group, 2019, FW5C.1.

[4] Manuj Singh et al. “Photonic molecule electro-optic modulators for efficient, widely tunable RF sideband generation and wavelength conversion”. In: *Frontiers in Optics + Laser Science 2021*. Optica Publishing Group, 2021, FTh6B.2.

[5] Ramy Rady et al. “A 20–43.5-GHz Wideband Tunable Silicon Photonic Receiver Front-End for mm-wave Channel Selection/Jammer Rejection”. In: *J. Lightwave Technol.* 41.5 (2023), pp. 1309–1324.

[6] Navid Hosseinzadeh et al. “A 0.5-20 GHz RF Silicon Photonic Receiver with 120 dB•Hz2/3 SFDR using Broadband Distributed IM3 Injection Linearization”. In: *2019 IEEE Radio Frequency Integrated Circuits Symposium (RFIC)*. 2019, pp. 99–102.